An Adaptive Mean-Shift Analysis Approach for Object Extraction and Classification From Urban Hyperspectral Imagery

Xin Huang and Liangpei Zhang

Abstract—In this paper, an adaptive mean-shift (MS) analysis framework is proposed for object extraction and classification of hyperspectral imagery over urban areas. The basic idea is to apply an MS to obtain an object-oriented representation of hyperspectral data and then use support vector machine to interpret the feature set. In order to employ MS for hyperspectral data effectively, a feature-extraction algorithm, nonnegative matrix factorization, is utilized to reduce the high-dimensional feature space. Furthermore, two bandwidth-selection algorithms are proposed for the MS procedure. One is based on the local structures, and the other exploits separability analysis. Experiments are conducted on two hyperspectral data sets, the DC Mall hyperspectral digital-imagery collection experiment and the Purdue campus hyperspectral mapper images. We evaluate and compare the proposed approach with the well-known commercial software eCognition (object-based analysis approach) and an effective spectral/spatial classifier for hyperspectral data, namely, the derivative of the morphological profile. Experimental results show that the proposed MS-based analysis system is robust and obviously outperforms the other methods.

Index Terms—Bandwidth selection, classification, high spatial resolution, hyperspectral, mean shift (MS).

I. INTRODUCTION

RECENTLY, the development and increasing use of images with both high spatial and spectral resolutions (namely, high spatial and spectral resolution (HSSR) imagery) have received more attention for land-cover/land-use mapping. Such HSSR data provide both detailed structural and spectral information; therefore, it should be useful for information extraction and classification. The application of HSSR images is a complex and challenging problem for the remote-sensing community. The key processing technique is the exploitation of the rich spectral and spatial features. Therefore, a joint spectral/spatial classifier is needed for the classification of this data, but few such approaches have been proposed [1]. Jackson and Landgrebe [2] presented an adaptive Bayesian contextual classifier to utilize spatial interpixel-dependence contexts, where the prior probabilities of the classes of each

pixel and its spatial neighbors are modeled by the Markov random field. In [3], Dundar and Landgrebe proposed a model-based mixture supervised-classification approach, in which a Gaussian mixture approach was used for accurate modeling of complex spectral classes. The mixture model was estimated using the expectation–maximization algorithm, and this approach was found substantially better than using only a single Gaussian density function (e.g., the maximum-likelihood classifier). Benediktsson *et al.* [1] proposed a mathematical morphology approach, namely, the derivative of the morphological profile (DMP), for preprocessing of HSSR imagery. The multiscale morphological profile is based on the repeated use of openings and closings with a structuring element of increasing size. The principal-component-analysis (PCA) transform is used to reduce the dimension and produce characteristic images for hyperspectral data, and the multiscale morphological features are then classified using the back-propagation (BP) neural networks. More recently, Gamba *et al.* [25] presented an improved very high resolution (VHR) urban-area mapping approach, where boundary and nonboundary pixels are separately classified using a fuzzy ARTMAP neural network and Markov random-field classifier, respectively. The labels in the boundary regions are then finely tuned by enforcing some geometrical constraints. A decision fusion is finally used to combine the two mapping outputs.

In this paper, a mean-shift (MS)-based analysis framework is proposed to extract spectral/spatial features from HSSR data. In this approach, the MS [4], [5] is used to obtain an object-oriented representation of hyperspectral imagery. Accordingly, several issues should be addressed.

1) Dimension Reduction for Hyperspectral Feature Space: On the one hand, it is necessary to reduce the computation load for HSSR data when spectral and spatial information are considered at the same time; on the other hand, the kernel density estimation in the MS does not scale well with high dimension of the space [5]. This is mostly due to the empty-space phenomenon [6] by which most of the mass in a high-dimensional space is concentrated in a small region of the space. Therefore, dimension-reduction algorithms are used for preprocessing of hyperspectral data and MS analysis. Several feature-extraction approaches have been tested for hyperspectral data: discriminant-analysis feature extraction [2], PCA [1], and independent component analysis [7]. In this paper, a relatively new feature-extraction algorithm, nonnegative matrix factorization (NMF) [8], is used to reduce the HSSR data and create characteristic images.

2) Object-Based Classification: The object-based-classification approaches can reduce the local spectral variation, generalize the spectral information in a spatial neighbor, and exaggerate the spectral distinction between spectrally similar objects. It has proven to be an efficient solution for VHR imagery [11], [12], [26]. Its basic idea is to group the spatially adjacent pixels into spectrally homogeneous objects and then conduct classification on objects as the minimum processing unit. Kettig and Landgrebe [27], [28] proposed this idea and developed the spectral–spatial classifier called extraction and classification of homogeneous objects. More recently, a commercial software eCognition [9] that exploits the object-based classification technique has been studied extensively and reported to be very effective for VHR data [10]–[12]. The key technique of eCognition is the fractal net evolution approach (FNEA) [9]. FNEA is a bottom-up region-merging approach starting from a single pixel. The region-merging decision is made with local homogeneity criteria. In an iterative way, at each subsequent step, image objects are merged into larger ones. FNEA can be regarded as a hierarchical segmentation that divides the data based on proximity measure. The hierarchical method tends to be computationally expensive, and the definition of a meaningful stopping criterion for the merging of the data is not straightforward [5]. Besides the hierarchical method, the density estimation is another efficient approach for feature-space clustering. MS is an elegant method of probability density estimation, and it is utilized for object-based classification in this paper. The rationale of the density-estimation-based segmentation approach is that the feature space can be regarded as the empirical probability density function (PDF). Local maxima of the PDF correspond to dense regions in the feature space, and their locations are used to delineate the local structure of data. MS is a robust feature-analysis technique for detail-preserving segmentation and, hence, is a very potential tool for object-based feature extraction and classification for high-resolution data.

3) Classifier: Support vector machine (SVM) has been reported to be effective in classification of multisensor data [29] and hyperdimensional object-based feature sets [10], [18]. It is not constrained to prior assumptions on the distribution of input data and is, hence, well suited for complex features. In this paper, SVM is used to interpret the HSSR data sets with MS-based object-oriented feature space.

The proposed framework is shown in Fig. 1. This paper aims to propose a novel MS-based object extraction and classification approach for HSSR imagery and to address some important issues for this application, including dimension reduction and adaptive bandwidth selection. The rest of this paper is organized as follows. Section II details the proposed adaptive MS analysis approach. Section III presents the MS-based object-oriented classification algorithm. Section IV analyzes and compares the experimental results. The last section concludes.

II. ADAPTIVE MS ANALYSIS APPROACH

A. MS Procedure

The MS is a nonparametric density-estimation technique, and its theoretical framework is the Parzen window-based
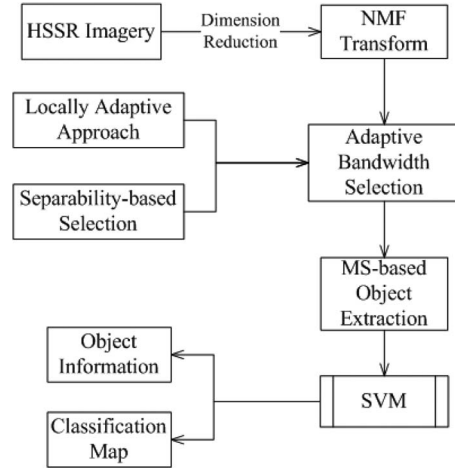

Fig. 1. MS system for object extraction and classification.

kernel density estimation [4], [5]. Given n data points x_i ($i = 1, \ldots, n$) in d-dimensional space, the kernel density estimator at point x can be written as

$$\hat{f}_{h,K}(x) = \frac{c_{k,d}}{nh^d} \sum_{i=1}^{n} k\left(\left\|\frac{x - x_i}{h}\right\|^2\right) \quad (1)$$

where $c_{k,d}$ is a normalization constant, h is the bandwidth, and $k(\cdot)$ is the kernel profile, that models how strongly the data points are taken into account for the estimation. The key step in the feature-space analysis is to find the local maxima of the density $f(x)$, i.e., the modes of the density, which are located among the zeros of the gradient $\nabla f(x) = 0$. The MS procedure is an efficient way to locate these zeros without estimating the density [5]. The density-gradient estimator can be obtained by differentiating (1) and decomposing to two product terms

$$\hat{\nabla} f_{h,K}(x) = \frac{2}{h^2 c} \hat{f}_{h,G}(x) \cdot m_{h,G}(x) \quad (2)$$

where the profile of kernel G is defined as $g(x) = -k'(x)$, with $c_{g,d}$ as its normalization parameter, and c is the normalization constant $c = c_{g,d}/c_{k,d}$. In (2), the first term is the density estimate at x with the kernel G

$$\hat{f}_{h,G}(x) = \frac{c_{g,d}}{nh^d} \sum_{i=1}^{n} g\left(\left\|\frac{x - x_i}{h}\right\|^2\right) \quad (3)$$

and the second term is the MS

$$m_{h,G}(x) = \frac{\sum_{i=1}^{n} x_i \cdot g\left(\left\|\frac{x - x_i}{h}\right\|^2\right)}{\sum_{i=1}^{n} g\left(\left\|\frac{x - x_i}{h}\right\|^2\right)} - x. \quad (4)$$

From (4), it can be found that the MS is the difference between the weighted mean, using the kernel G for weights, and x, the center of the kernel. According to (2), the MS can be written as

$$m_{h,G}(x) = \frac{1}{2} h^2 c \frac{\hat{\nabla} f_{h,K}(x)}{\hat{f}_{h,G}(x)}. \quad (5)$$

Equation (5) shows that the MS vector at point x with kernel G is proportional to the normalized density-gradient estimate obtained with kernel K, and it thus always points toward the direction of maximum increase in the density. In other words, the local mean is shifted toward the region in which the majority of the points reside [5].

Remote-sensing imagery is typically represented as a spatial-range joint feature space. The spatial domain denotes the coordinates and locations for different pixels, and the range domain represents the spectral signals for different channels. The multivariate kernel is defined for joint density estimation

$$K(x) = \frac{C}{h_s^2 h_r^p} \prod_{u \in \{s,r\}} k \left(\left\| \frac{x^u}{h_u} \right\|^2 \right) \qquad (6)$$

where C is a normalization parameter and h_s and h_r are the kernel bandwidths for spatial and range subdomains. The dimensionality of the joint domain is $d = 2 + p$ (two for spatial domain and p for spectral domain). Based on the earlier statements, two issues should be addressed when MS analysis is implemented on remotely sensed imagery. First, due to the empty-space phenomenon by which most of the mass in a high-dimensional space is concentrated in a small region of the space [5], the density should be analyzed along lower dimensionality. Second, since the MS feature-space analysis is task-dependent, the kernel bandwidths should be determined by different applications. Therefore, in this paper, the NMF algorithm is employed for reducing the dimension of hyperspectral features. On the other hand, two adaptive bandwidth-selection approaches are proposed by exploiting the separability between spectrally similar classes and the locally structural features.

B. Hyperspectral Dimension Reduction Using NMF

NMF is a parts-based learning algorithm and is an efficient decomposition approach for statistical analysis of multivariate data. This is in contrast to other methods, such as PCA and vector quantization, which learn holistic, not parts-based, representations [8]. NMF is distinguished from the other methods by its use of nonnegativity constraints. These constraints lead to a parts-based representation because they allow only additive, not subtractive, combinations. Given a nonnegative matrix V, the task of NMF is to find two matrices W and H with nonnegative elements such that

$$V \approx WH. \qquad (7)$$

One natural way to solve the NMF problem is to formulate an optimization problem by minimizing the distance between V and WH

$$\text{minimize } f(W, H) = \|V - WH\|$$
$$\text{subject to } W \geq 0 \quad H \geq 0. \qquad (8)$$

The constrained problem is resolved by an iterative learning algorithm that preserves the nonnegative property of W and H and also constrains the columns of W to sum to unity. Presumably, the columns of W represent the latent variables,

i.e., physically meaningful nonnegative "parts" of the underlying data. The parts-based characteristic has found NMF a wide range of applications in data analysis, dimensionality reduction, and feature extraction [14]. In this paper, NMF is used for preprocessing of MS analysis and feature extraction from hyperspectral data. Detailed reviews of the algorithm can be found in [8].

C. Adaptive Bandwidth Selection for MS Analysis

The major challenge for applying the MS algorithm to remote sensing is that the bandwidths in the spatial and spectral domains need to be adaptively determined. In [19], the spatial-domain bandwidth is set to $h_s = \max\{4, \min\{\text{height}, \text{width}\}/100\}$, and the spectral domain window width is $h_r = 5$. In [6], Fukunaga proposed that the bandwidth-selection technique should be related to the stability of the decomposition. The bandwidth is taken as the center of the largest operating range over which the same number of clusters are obtained. In [20], Comaniciu proposed a variable-bandwidth technique that imposes a local structure on the data to extract reliable scale information. The local bandwidth is obtained by maximizing the magnitude of the normalized MS vector. However, finally, since in most of the cases the MS-based decomposition is task-dependent, the information provided by a user or by a specific problem should be used to control the kernel bandwidth. Therefore, in this paper, we propose two algorithms to adaptively select bandwidth parameters for remote-sensing image classification and object recognition. One is based on the separability in feature space, and the other exploits local homogeneity.

1) Algorithm 1: Separability-Based Bandwidth Selection:

1) Define a set of bandwidths $\{h_s(1), \ldots, h_s(t), \ldots, h_s(T)\}$ and $\{h_r(1), \ldots, h_r(t), \ldots, h_r(T)\}$ for spatial and range domains, respectively. Different MS-based features are obtained using different bandwidth parameters.
2) The Jeffries–Matusita (JM) distance [21] is used to measure the separability of the feature space with different bandwidths. The values of the JM distance indicate how well the selected class pairs are statistically separate. A high value indicates that the feature space can be well separated, while a low value indicates that the feature space is not well separated. The JM index was originally designed for a two-class problem

$$J_{ij} = \int_x \left[\sqrt{p(x/C_i)} - \sqrt{p(x/C_j)} \right]^2 dx \qquad (9)$$

where $p(x/C_i)$ and $p(x/C_j)$ are the conditional PDFs of feature vector x for classes C_i and C_j, respectively. In this paper, a multiclass JM index is used to measure the separability [22]

$$J = \sum_{i=1}^{C} \sum_{j>i}^{C} \sqrt{p(C_i)p(C_j)} J_{ij}^2 \qquad (10)$$

where $p(C_i)$ and $p(C_j)$ are the *a priori* class probabilities. It is worth noting that, in this paper, the JM index is computed between the least separable class pairs (spectrally similar classes). For the set of spatial bandwidths, the corresponding JM indexes are written as $(J(1), \ldots, J(t), \ldots J(T))$.

3) The optimal bandwidth values are automatically determined when the JM distances stably increase to high values. This criterion is defined as

$$\left.\begin{array}{l} |J(t+1) - J(t)| < \varepsilon \\ |J(t+2) - J(t+1)| < \varepsilon \end{array}\right\} \Rightarrow h_s = h_s(t) \qquad (11)$$

where ε is a small positive constant (in this paper, 0.015).

4) Repeat 2) and 3) for the range scales $\{h_r(1), \ldots, h_r(t), \ldots, h_r(T)\}$ to select the suitable range bandwidth h_r.

2) Algorithm 2: Local Homogeneity-Based Bandwidth Selection: The basic idea of this algorithm is to search for the latent modes in a homogeneous area. To this end, the pixel-shape index (PSI) [23] is used to measure the spatial structures and estimate the spatial bandwidth for each pixel. PSI is computed pixel by pixel by searching along a predetermined number of equally spaced lines (direction lines) radiating from the central pixel. It aims to examine the context of each pixel, and its value represents the spatial dimensions of groups of spectrally similar connected pixels. D-direction lines can be determined for each pixel x_i, and the direction-lines histogram is defined as $H(x) : \{x \in I | [L_1(x), \ldots L_d(x), \ldots L_D(x)]\}$, where $L_d(x)$ is the length of the dth direction line. The PSI-based bandwidth estimation can be modeled using an improved version of (1)

$$\hat{f}_K(x) = \frac{c_{k,d}}{n[h(x)]^d} \sum_{i=1}^{n} k\left(\left\|\frac{x - x_i}{h(x)}\right\|^2\right)$$

with

$$2h(x) + 1 = \text{PSI}(x) = \frac{1}{D}\sum_{d=1}^{D} L_d(x) \qquad (12)$$

where $h(x)$ denotes the bandwidth for each estimation point x. In such way, the spatial scale is determined according to the averaged diameter of the homogeneous region around the current point. In (12), it should be noticed that PSI denotes the diameter of the homogeneous region, and $h(x)$ is the radius.

Comparing algorithms 1 and 2, the first one selects the optimal parameters for the whole image according to class separability, and the other one chooses the suitable parameter for each estimation point according to local structure and homogeneity.

III. MS-BASED CLASSIFICATION SYSTEM

MS is an efficient spatial-feature-extraction approach that is capable of delineating arbitrarily shaped clusters due to its non-parametric nature. It can exploit contextual homogeneity and reduce spectral variation in a local area and, at the same time, preserve edge and detailed information. This characteristic has
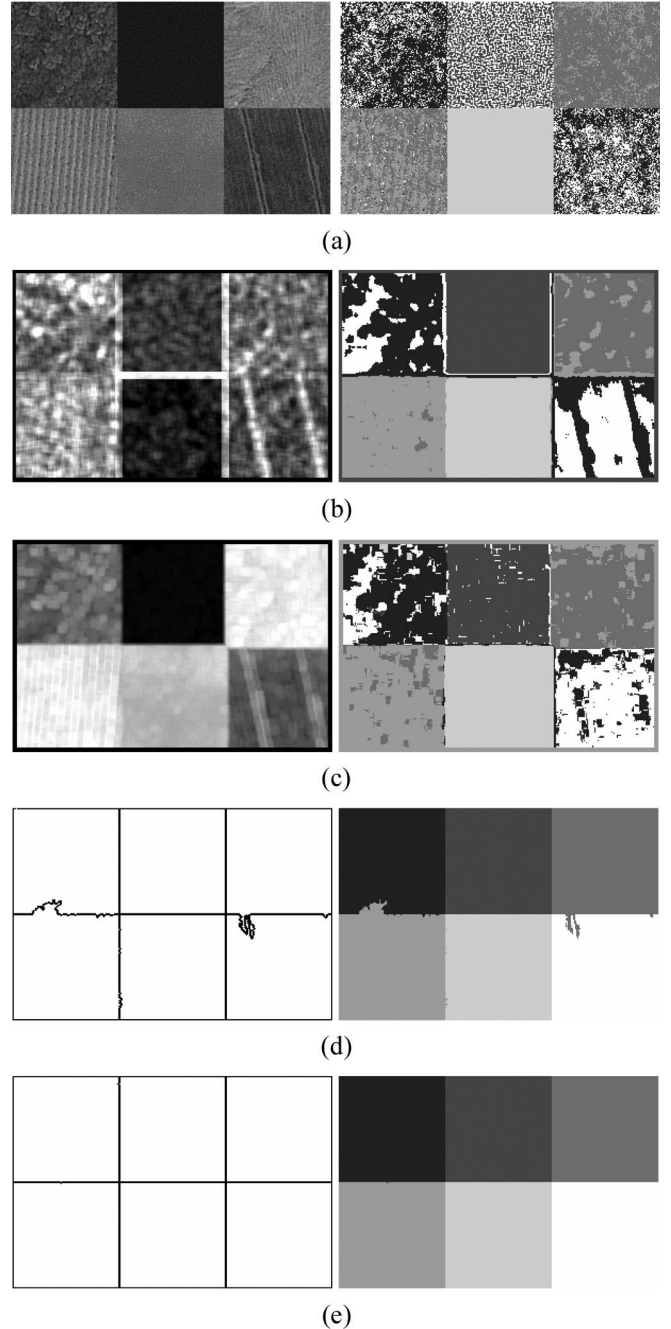

(a)

(b)

(c)

(d)

(e)

Fig. 2. Feature images and classification results for different algorithms. (a) Texture test image and the result of spectral classification. (b) GLCM feature image and its classification result. (c) OWT feature image and its classification result. (d) FNEA segmentation image and its classification result. (e) MS segmentation image and its classification result.

found MS a potential tool of spatial feature extraction and segmentation/classification for high-resolution imagery. The proposed MS-object-based classification algorithm consists of the following steps.

1) Let $x = \{x^b\}_{b=1}^{B}$ $(x \in I)$ be the input of dimensionally reduced hyperspectral data with I representing the whole image and B the number of spectral channels. Let $y = \{y^b\}_{b=1}^{B}$ be the values at point x after the MS procedure.

2) Initialize $j = 1$ and $y_1 = x$ with j denoting the current number of MS iterations $(1 \le j \le c)$. Compute the MS

(a)   (b)   (c)

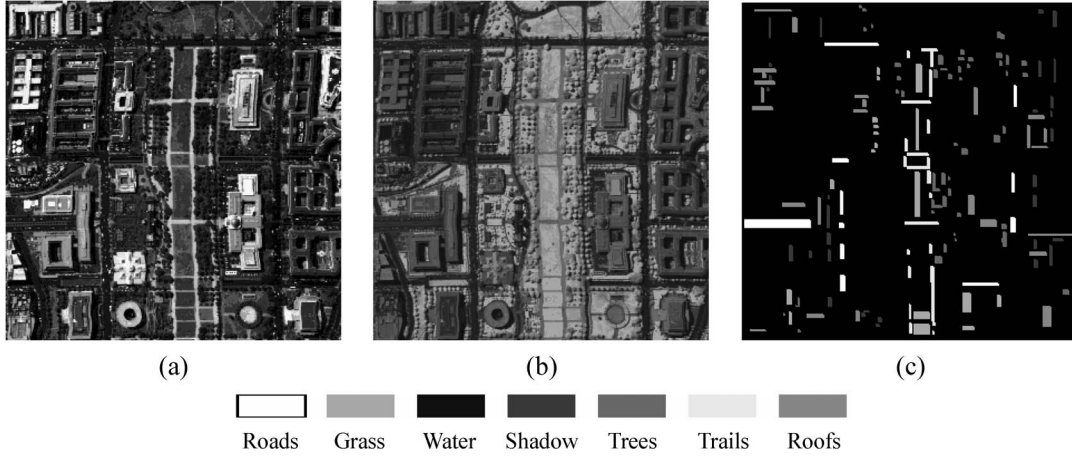Roads   Grass   Water   Shadow   Trees   Trails   Roofs

Fig. 3.   HYDICE experiment 1 with NMF spectral features and test samples. (a) Image for test 1. (b) NMF feature image 1. (c) Test samples 1.

vector until convergence

$$m_{h,G}(y_j) = y_{j+1} - y_j. \tag{13}$$

The MS vector defines a path leading to stationary points of the density (i.e., modes), and the kernel in the MS procedure moves in the direction of the maximum increase in the density gradient. The MS iterations are large in low-density regions and small near local maxima. We define $y = y_c$, where y_c represents the weighted mean in the convergence point y

$$y = y_c = \frac{\sum\limits_{x_i \in S(y_c)} x_i \cdot g\left(\left\|\frac{y_c - x_i}{h(y_c)}\right\|^2\right)}{\sum\limits_{x_i \in S(y_c)} g\left(\left\|\frac{y_c - x_i}{h(y_c)}\right\|^2\right)} \tag{14}$$

where $S(y_c)$ represents the set of points satisfying the condition $\text{dist}(x_i, y_c) < h(y_c)$ with the function $\text{dist}(\cdot)$ being the distance between two vectors.

3) The segmentation results are obtained by postprocessing of the MS procedure. The modes at a distance less than the kernel bandwidth are fused, the one corresponding to the highest density being chosen (i.e., the significant mode). Each image object is the set of points that converge to the same significant mode.

4) Calculate the averaged values of pixels in each object at band b: z^b, and let C_l ($1 \leq l \leq L$) be an information class in an image. Accordingly, $x = \{x^b\}_{b=1}^B$ and $z = \{z^b\}_{b=1}^B$ represent pixel-based and object-based feature vector for each classification unit. The classification rule can be written as follows:

Pixel-based classification :
$$x \in C_l \Leftrightarrow \text{Cla}(x) = C_l \tag{15}$$

Object-based classification :
$$z \in C_l \Leftrightarrow \text{Cla}(z) = C_l \tag{16}$$

where $\text{Cla}(\cdot)$ is the decision result using a classifier.

TABLE I
NUMBERS OF TRAINING AND TEST SAMPLES FOR
THE TEST IMAGE 1 IN THE DC DATA SET

Information Classes	No. of Training Samples	No. of Test Samples
Roads	55	892
Grass	57	910
Shadow	50	567
Trails	46	624
Trees	49	656
Roofs	52	1,123
Total	309	4,772

An experiment of texture segmentation is provided in this paper to demonstrate the performance of MS for high-resolution remotely sensed imagery. A QuickBird true-color image of Beijing with six different texture features is employed for this test. Fig. 2(a) shows a mosaic of the six different land-cover types, coded as C1 to C6 from left to right and then up to bottom. C1, C2, and C3 are woodlands, water body, and bare soil, respectively. C4 and C6 are different kinds of crops, and C5 is grassland. C3 and C4 are spectrally similar, and C1, C5, and C6 are similar. Five algorithms are used and compared for recognition of the texture image: spectral classification, gray-level cooccurrence matrix (GLCM) [15], overcomplete wavelet transform (OWT) [16], FNEA segmentation [17], and the MS-based approach. The results are shown in Fig. 2.

In Fig. 2, results (a), (b), and (c) are obtained by supervised classification of the respective feature images, while results (d) and (e) are computed using unsupervised segmentation with six clusters. The spectral classifier in (a) shows obvious misclassification because of similar spectral responses between different classes, and pepper–salt effect can be observed due to the pixel-based approach. GLCM and WT are commonly used spatial-feature measures in remote sensing and have proven to be efficient for texture recognition [18]. However, their disadvantages are apparent when they are applied to high-spatial-resolution images. The moving window sizes may not favor all the land-cover types, and usually, they have blur effects in border regions and cannot delineate accurate results at the boundaries of different land-cover units. Much better results are obtained in (d) and (e), although an unsupervised classification
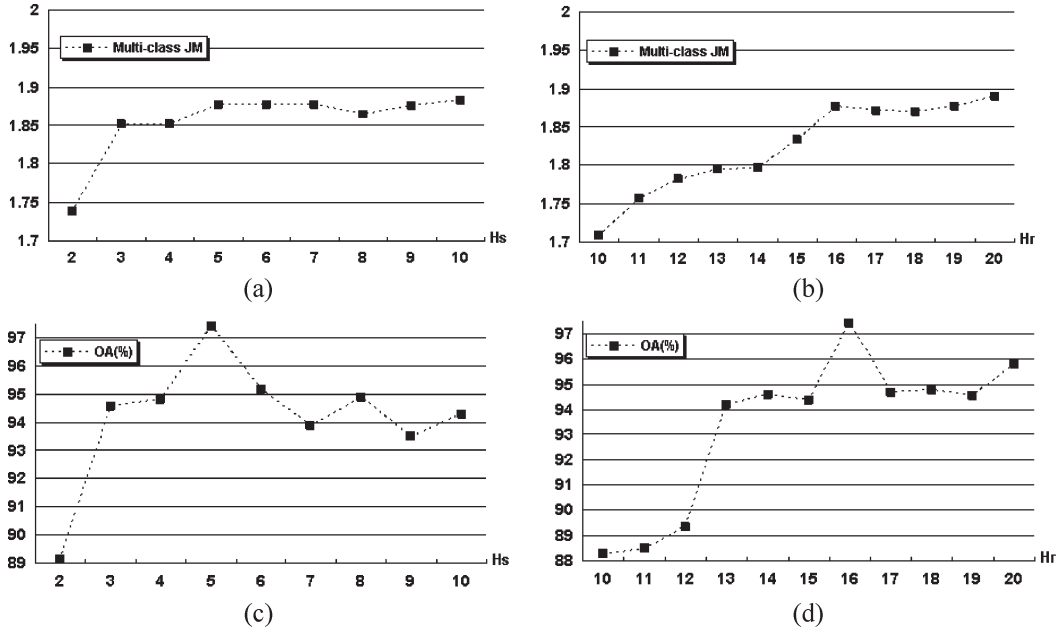
(a)

(b)

(c)

(d)

Fig. 4. (a) and (b) Relationship between the multiclass JM index and the spatial and range bandwidths, respectively. (c) and (d) Classification accuracies for different spatial and range parameters, respectively. It should be noticed that the statistical results in (a) and (c) are obtained with different spatial bandwidths while keeping $h_r = 16$, and results in (b) and (d) are obtained with different range bandwidths while keeping $h_s = 5$.
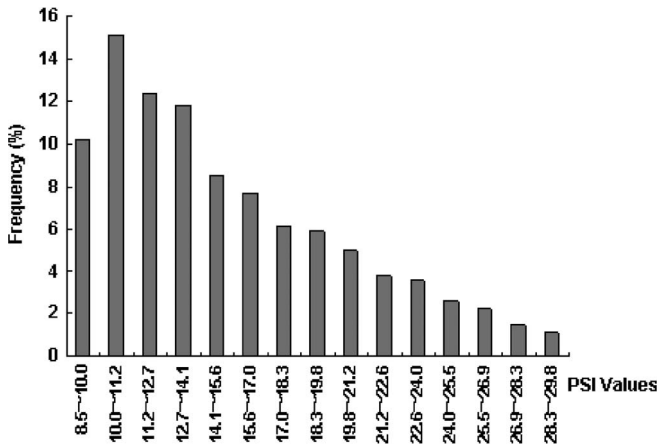

Fig. 5. PSI histogram for test area 1.

is utilized, which shows that the object-based method is a better alternative to the traditional pixel-based methods for high-resolution data. It is worth noting that MS-based method achieves nearly perfect segmentation, and it accurately locates edge pixels and homogeneous areas. This experiment shows the potential of MS for object-based analysis.

IV. EXPERIMENTS, ANALYSIS, AND COMPARATIVE STUDY

The objective of the experiments is to apply MS analysis to object extraction and classification for HSSR data and to conduct a comparative study between the MS-based approach, eCognition-based classification [9], and the multiscale DMP algorithm [1].

A. Study Area

The experiments are conducted on two hyperspectral data sets. One is the hyperspectral digital-imagery collection ex-
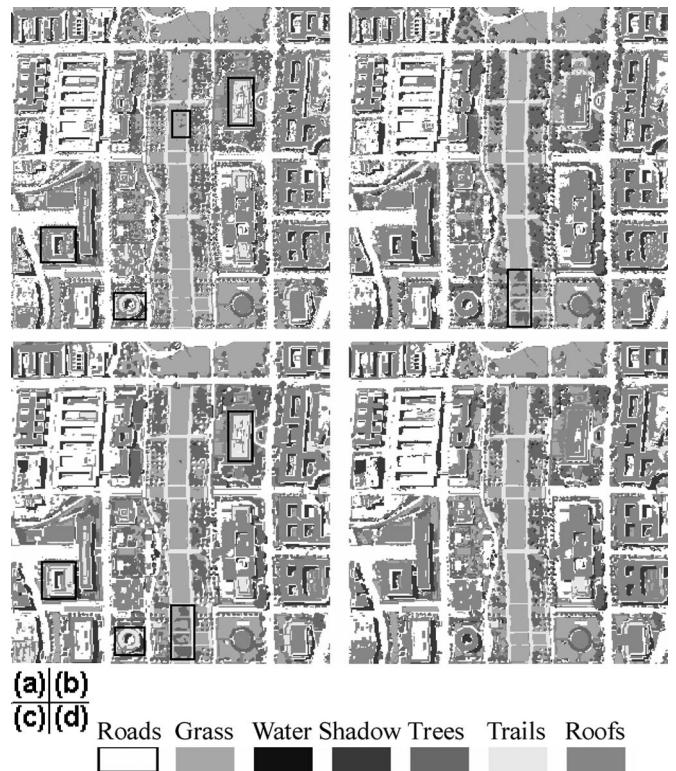

Fig. 6. (a)–(d) Classification maps obtained using spectral classification (OA = 89.4%), DMP features (OA = 93.4%), FNEA approach (OA = 89.6%), and MS-based approach (OA = 97.2%), respectively. Some detailed results are highlighted in black rectangles.

periment (HYDICE) airborne hyperspectral data flight over the Mall in Washington, DC [24]. In the 0.4–2.4-μm region, 210 bands were collected of the visible and infrared spectrums. The water-absorption bands were then deleted, resulting in 192 channels. This data set contains 1280 scan lines with

307 pixels in each scan line. It totals approximately 150 MB. The other is a flight over the West Lafayette campus of Purdue University [24]. The hyperspectral data were collected on September 30, 1999 with the airborne hyperspectral mapper (HYMAP) system, providing image data in 126 spectral bands in the visible and infrared channels (0.4–2.4 μm).

B. Experiments for Washington, DC, Data 1

Two subsets of the DC data are shown in Figs. 3(a) and 7(a). The desired information classes are *Roads, Grass, Water, Trails, Trees, Shadow*, and *Roofs*. The DC data set is a challenging one to analyze for several reasons. First, classes are complex. There is a large diversity in the materials used in constructing rooftops, and consequently, no single spectral response is representative of the class *Roofs*. Second, *Roofs, Roads*, and *Trails* are spectrally similar in that they may be made of similar materials. At the same time, *Shadow* and *Water* are quite similar so that they cannot be discriminated effectively using spectral signals. Third, the data were collected during the dry season; most lawns are not well grown, and as a result, the classes *Grass* and *Trails* are difficult to differentiate, since some areas of grass are nearly bare soil, which is spectrally similar to the gravel of *Trails*.

The first test data are shown in Fig. 3(a). The training and test samples are listed in Table I, and the test regions are shown in Fig. 3(c). Fig. 3(b) shows the 3-D NMF feature image ($B = 3$), which is extracted from the 192-channel hyperspectral data. The least separable class pairs are selected as follows: *Trails–Roofs, Roads–Shadow*, and *Grass–Trees* due to their similar spectral responses. The optimal bandwidths are determined as follows: $h_s = 5$ and $h_r = 16$ according to (11). The multiclass JM indexes [(10)] as a function of different spatial and range bandwidths are shown in Fig. 4.

From Fig. 4(a), it is shown that a small spatial window (e.g., $h_s = 2$) leads to a low JM index. MS is a probability-density-estimation approach, and hence, a very small window size is not reasonable for statistical analysis. When h_s increases, the feature space becomes more separable, and the JM values become stable with $h_s \geq 5$. It is worth noting that, when larger window sizes are used for spatial bandwidths, the JM distance fluctuates and does not improve much. Considering that more convergence time is needed for a larger spatial bandwidth, therefore, the parameter selection is a tradeoff between robust estimator and computational load. The *Algorithm 1* is an efficient approach to address this problem because it searches for the optimal parameter by computing the JM indexes from small bandwidths to large ones until the separability becomes stable. Additionally, the variable bandwidth selection using *Algorithm 2* is shown in Fig. 5, where the PSI histogram for the test image 1 is shown. It can be found that the most frequent PSI values are between 10.0 and 11.2, corresponding to $h_s = 5$.

Fig. 3(a) is classified with different parameters to test the bandwidth-selection algorithms. The classification results are evaluated using two statistical measures, overall accuracy (OA) and Kappa coefficient, based on the confusion matrix. Results are shown in Fig. 4(c) and (d) for different spatial and range parameters, respectively. The experimental re-

TABLE II
CLASSIFICATION ACCURACIES FOR FNEA AND MS APPROACHES
WITH DIFFERENT NUMBERS OF OBJECTS

	No. of Objects	OA (%)	Kappa	Time (s)
FNEA	2,269	89.3	0.871	3.5
	7,035	89.6	0.875	2.7
	7,954	89.4	0.872	2.4
	8,359	89.5	0.873	2.0
MS	2,286	93.6	0.922	3.3
	7,032	97.2	0.965	2.2
	8,007	94.8	0.937	1.6
	8,326	94.3	0.932	1.7

TABLE III
CLASS-SPECIFIC ACCURACIES FOR THE FOUR
CLASSIFICATION MAPS SHOWN IN FIG. 6

	NMF	DMP	FNEA	MS
Roads	94.9	95.6	95.2	95.6
Grass	86.1	89.2	86.7	99.2
Shadow	96.4	97.6	97.4	98.1
Trails	88.1	96.9	88.0	97.0
Trees	86.0	88.7	86.1	99.1
Roofs	90.1	95.9	89.7	95.5
AA (%)	90.3	94.0	90.5	97.4
OA (%)	89.4	93.4	89.6	97.2

sults are interesting in that the bandwidths ($h_s = 5$, $h_r = 16$) selected by *Algorithm 1* achieve the highest accuracy (97.4% for OA and 0.968 for Kappa). It can be seen that larger bandwidths do not necessarily result in better results due to the oversmoothed effects for larger windows. The figure also shows that the multiclass JM index is effective in choosing the appropriate parameters. On the other hand, the accuracies for the PSI-based bandwidths (*Algorithm 2*) are 97.2% for OA and 0.965 for Kappa. In spite of slightly lower accuracies, the PSI approach succeeded in determining proper bandwidths for each pixel based on locally structural information. The PSI histogram for data set 1 is shown in Fig. 5, and its classification map is shown in Fig. 6(d).

Four different features are compared in Fig. 6. Fig. 6(a)–(d) is obtained using NMF-based spectral classification, 21-D DMP features (including 18-D morphological profiles and three-band NMF features), FNEA-based classification, and the proposed MS-based approach. The dimensions of FNEA and MS features are both three. All the features are classified using the SVM classifier with the radial-basis-function (RBF) kernel [13], which has been proven effective in a number of different classification problems [10].

In Fig. 6, the MS-based classification obtained the best results in both accuracies and visual interpretation. In these maps, two spectrally similar class pairs, *Roofs–Trails* and *Grass–Trees*, are focused on. From Fig. 6(a), it is shown that the pixel classification results in obvious pepper and salt effects in homogeneous regions such as roads, grass lands, and roofs. Furthermore, pixel-based method cannot discriminate the spectrally similar classes. The DMP algorithm achieved good results except for some misclassifications between *Grass*
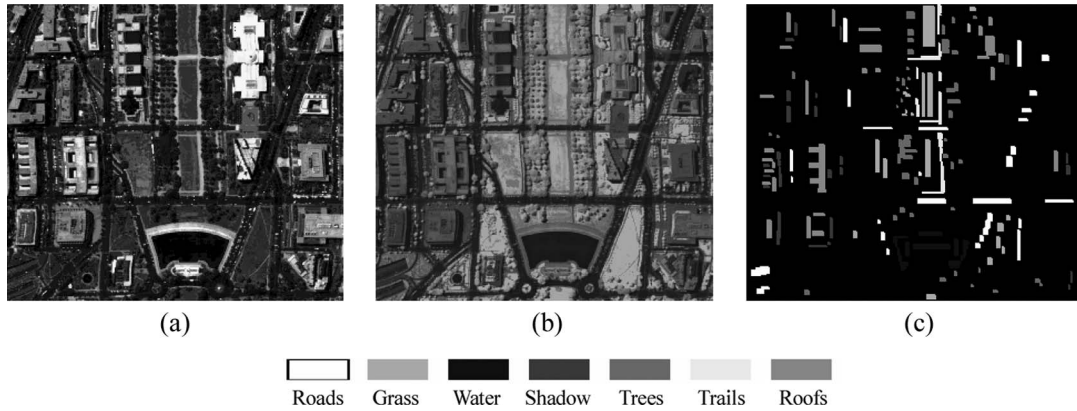
Fig. 7. HYDICE experiment 2 with NMF spectral features and test samples (the legend is the same as that in Fig. 3). (a) Image for test 2. (b) NMF feature image 2. (c) Test samples 2.

and *Trees* because it integrates multiscale structural features and multispectral information. It should be noticed that the spectral classification, FNEA-based classification, and MS-based approach only employ 3-D features, while the DMP algorithm includes 21-D features. In order to evaluate FNEA and MS approaches roundly, their classification accuracies with different segmentation scales are compared in Table II.

From Table II, it is shown that the MS approach outperformed FNEA when images were segmented with similar scales. Furthermore, the CPU time for segmentation of the MS approach is comparable or less than that of FNEA. The MS classification provides stable accuracies with OA higher than 93.5% and Kappa larger than 0.92. FNEA segmentation is a hierarchical clustering technique that divides the data based on homogeneity, while MS is a clustering approach according to local maxima of the PDF. The experimental results for test area 1 show the superiority of the MS approach for object-based classification. This conclusion is also verified in the class-specific accuracies of the maps shown in Fig. 6, which are provided in Table III (AA denotes the averaged accuracies of different classes).

C. Experiments for Washington, DC, Data 2

The other subset of HYDICE DC data are tested for the proposed method and the comparative study. The test data 2 is shown in Fig. 7, and the training and test samples are listed in Table IV. The spectrally similar class pairs in this test area include *Roads–Shadow*, *Water–Shadow*, and *Trails–Roofs*, and they are selected for the bandwidth estimation using **Algorithm 1**. The relationships between the multiclass JM distance and the bandwidth values are shown in Fig. 8(a) and (b), respectively.

According to (11), the optimal bandwidths are set to $h_s = 4$ and $h_r = 16$. From Fig. 8, it is shown that the range bandwidths influence the JM indexes and classification accuracies very much but the spatial bandwidths do not. In Fig. 8(d), it is shown that there is a sharp increase of OA from $h_r = 15$ to $h_r = 16$ (87.8%–98.4%) and then the accuracies become invariable, and it is interesting to see that, in Fig. 8(b), there is also an obvious increase of JM distance from $h_r = 15$ to $h_r = 16$ (1.25–1.35), and then, the JM indexes become stable. The results from the

TABLE IV
NUMBERS OF TRAINING AND TEST SAMPLES FOR
THE TEST IMAGE 2 IN THE DC DATA SET

Information Classes	No. of Training Samples	No. of Test Samples
Roads	63	1,090
Grass	62	1,082
Water	59	403
Trails	59	469
Trees	60	734
Shadow	61	461
Roofs	60	1,292
Total	424	5,531

two data sets show that the multiclass-JM-index-based algorithm can detect the suitable range of bandwidths. The JM index is an efficient task-dependent approach for adaptive bandwidth selection, since it considers the separability of spectrally similar class pairs.

Fig. 9 shows the relationship between bandwidth and the number of segmented objects for the two data sets. It can be observed that the number of objects tends to be stable when spatial bandwidth increases. This is because the spatial bandwidth represents the local variations near a significant mode (maxima of PDF), and its value determines the number of potential modes. That is the reason why some bandwidth-selection techniques are related to the stability of the decomposition, and the bandwidth is taken as the center of range over which the same number of clusters is obtained. In this paper, we do not employ this strategy for bandwidth selection, since the proposed JM measure is more effective for classification, which is a task-dependent problem. From Fig. 9(c) and (d), we can see a nearly linear descent of the number of objects with increasing range bandwidths, and the two curves do not show a stable tendency even when the number of objects decreases from 11 000 to 2500. Therefore, the bandwidth in the range domain cannot be determined according to the stability of the decomposition. In this paper, we consider the range bandwidth as a scale factor for classification and utilize the JM measure for an adaptive estimation.

Again, the classification maps for the four different features are compared. Fig. 10(a)–(d) are obtained using NMF-based spectral classification, 21-D DMP features, FNEA approach,
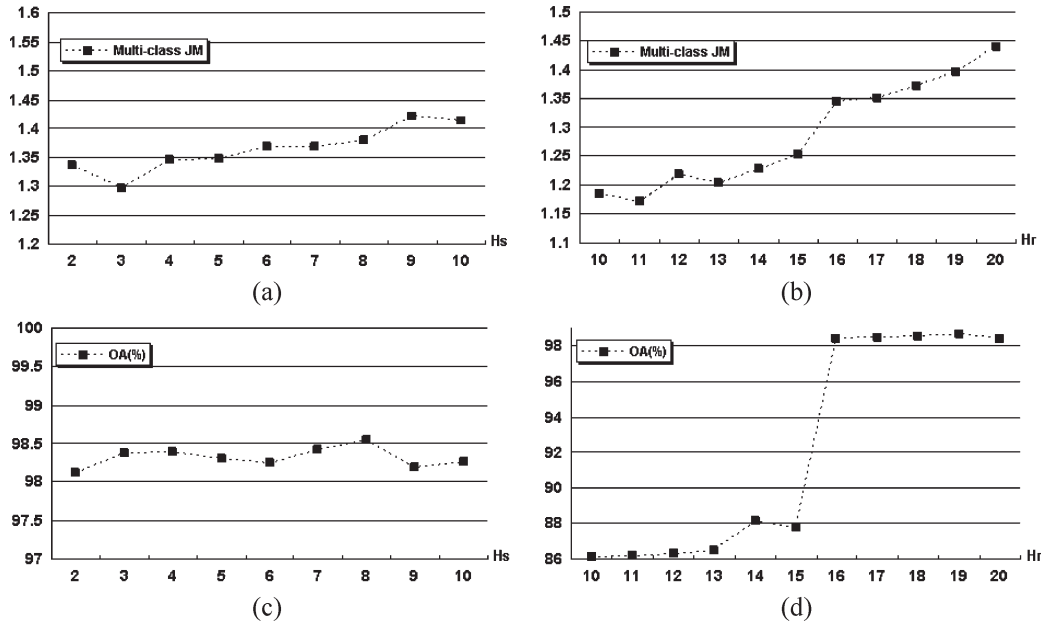
Fig. 8. (a) and (b) Relationship between the multiclass JM index and the spatial and range bandwidths, respectively. (c) and (d) Classification accuracies for different spatial and range parameters, respectively. It should be noticed that the statistical results in (a) and (c) are obtained keeping $h_r = 16$, and results in (b) and (d) are obtained keeping $h_s = 4$.
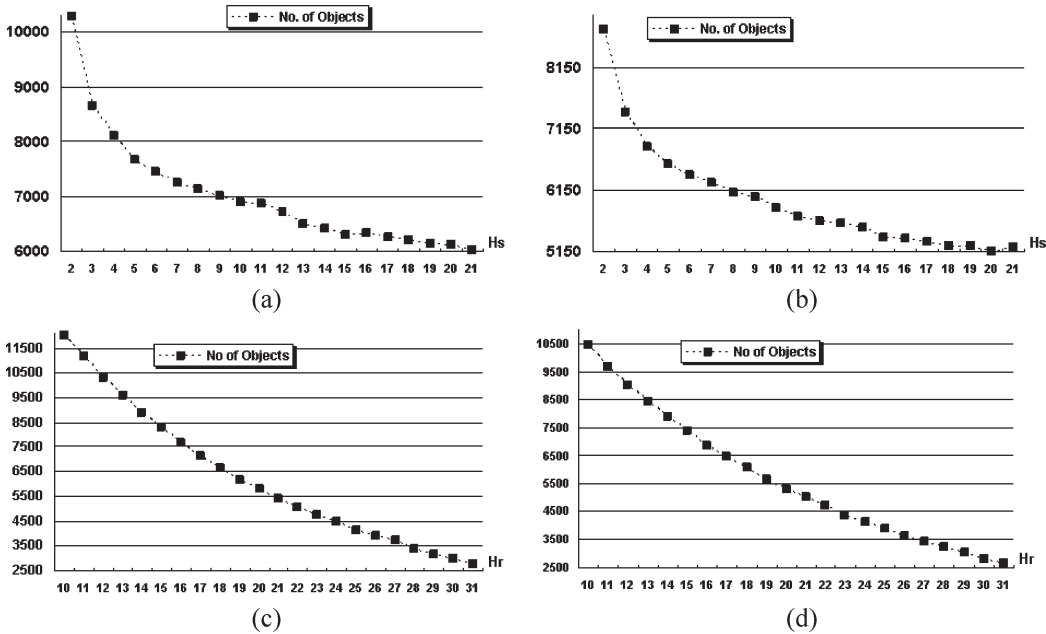

Fig. 9. (a) and (b) Spatial bandwidths as the function of the number of segmented objects for DC data sets 1 and 2, respectively. (c) and (d) Relationship between the range bandwidths and the number of objects for data sets 1 and 2, respectively.

and the MS-based classification. SVM classifier with RBF kernel is used for all the feature sets. It is worth noting that the PSI-based bandwidth selection is used for the MS procedure, and adaptive parameters are determined for each pixel, which leads to 6558 objects. For a fair comparison, the FNEA algorithm is implemented for segmentation with 6533 objects. From Fig. 10, it can be observed that the spectral classification cannot discriminate the spectrally similar classes such as *Trails–Roofs* and *Water–Shadow*. The result of high-dimensional DMP features, which combine spectral and structural information, obviously improves the spectral method. Comparing the results of DMP

and MS, it can be found that the MS approach is more effective in delineating the shape and structures and avoids pepper and salt effects. Table V is provided to evaluate FNEA and MS approaches, and their classification accuracies with different numbers of objects are compared. The results in Fig. 10 and Table V show that the MS is a more robust and efficient approach for object-based analysis than FNEA.

The class-specific accuracies are shown in Table VI. It can be seen that the proposed MS approach obtained the highest accuracies for all the information classes. It concludes that the MS-based approach can exploit the rich spectral and spatial

(a)(b)
(c)(d)

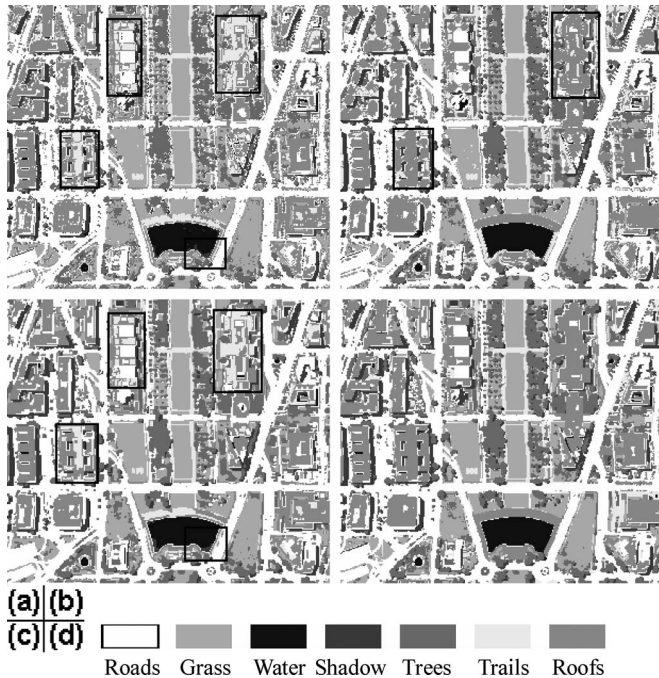Roads Grass Water Shadow Trees Trails Roofs

Fig. 10. (a)–(d) Classification maps obtained using spectral classification (OA = 85.7%), DMP features (OA = 95.8%), FNEA approach (OA = 87.6%), and MS-based classification (OA = 98.4%), respectively. Some detailed results are highlighted in black rectangles.

TABLE V
CLASSIFICATION ACCURACIES FOR FNEA AND MS APPROACHES
WITH DIFFERENT NUMBERS OF OBJECTS IN TEST 2

	No. of Objects	OA (%)	Kappa	Time (s)
FNEA	3,825	88.8	0.868	2.9
	5,764	89.2	0.871	2.5
	6,029	89.2	0.872	2.3
	6,533	87.6	0.853	2.1
	7,413	87.6	0.853	2.0
MS	3,859	97.6	0.971	1.8
	5,802	98.6	0.983	1.0
	6,071	98.5	0.982	0.9
	6,558	98.4	0.981	0.9
	7,422	98.4	0.980	0.7

TABLE VI
CLASS-SPECIFIC ACCURACIES FOR THE FOUR
CLASSIFICATION MAPS SHOWN IN FIG. 10

	NMF	DMP	FNEA	MS
Roads	94.8	95.9	94.6	97.1
Grass	99.7	99.4	100	100
Water	85.2	95.8	88.3	96.1
Trails	71.1	89.6	73.2	100
Trees	99.5	99.4	99.9	99.9
Shadow	82.7	92.1	84.6	93.8
Roofs	76.2	95.1	79.6	99.3
AA (%)	87.0	95.3	88.6	98.0
OA (%)	85.7	95.8	87.6	98.4

information in HSSR data at the same time, and it is suitable for different objects and classes with different scales and sizes.

D. Experiments for Purdue Campus Data Set

Another HSSR data set of the HYMAP campus is tested in order to verify that the algorithm performs well in a stable manner. Three-dimensional spectral features are extracted from the original 126-bands HYMAP data [Fig. 11(a)], and they are used for basis images of spatial feature extraction and object-based classification. Four features are compared: spectral feature, FNEA approach, combination of spectral and spatial information [23], and the MS-based method. Table VII provides the numbers of training and test samples, and Fig. 11 shows their classification maps. The class-specific accuracies are listed in Table VIII. It should be noted that the numbers of segmented objects are, respectively, 15 228 and 15 361 for FNEA and MS approaches for a fair comparison.

From Fig. 11 and Table VIII, it can be found that the spectral method cannot achieve a satisfactory classification, particularly for some spectrally similar classes such as *Roads* and *Roofs*. The purely spectral classification was improved when spatial information is added in the feature space. The combination of NMF images and PSI features obtained higher accuracies as compared to the spectral approach. The improvements in AA and OA are 7.8% and 9.0%, respectively. As for the object-based method, MS outperformed FNEA for all the information classes, and the respective improvements in AA and OA are 4.2% and 3.8%. In order to further compare the four algorithms, we extract the road information from the four maps shown in Fig. 11, and their results are shown in Fig. 12. The road extraction is based on the classification map, and the postprocessing includes centerline extraction and connected component analysis (CCA). The road centerline is extracted by performing a thinning algorithm on the binary road objects, and CCA is then used to remove small branches shorter than a user-defined threshold. The results in Fig. 12 show that the MS-based approach obtained the most accurate road information, and the roads shown in Fig. 12(d) appear more continuous and regular, and most of the noise segments are deleted.

V. CONCLUSION

This paper proposed a novel MS system for urban mapping using hyperspectral imagery with high spatial resolution. MS is a robust feature-space-analysis approach that can effectively locate the modes (local maxima of probability density) in the image. In this paper, it is used for object extraction by considering its advantages to the hierarchical methods (e.g., FNEA). In order to apply MS to hyperspectral image processing, the NMF is first used to reduce the dimensionality of the data and avoid the empty-space phenomenon by which most of the mass in a high-dimensional space is concentrated in a small region of the space. Density can then be analyzed within a lower dimensional subspace. Another key technique for MS is the adaptive bandwidth selection. In this paper, we proposed two approaches to adaptively determine the bandwidth parameters. The first is a task-dependent method that exploits the separability of spectrally similar class pairs (multiclass JM distance). The optimal bandwidth is selected when the JM index becomes stable. The other algorithm aims to find the modes in
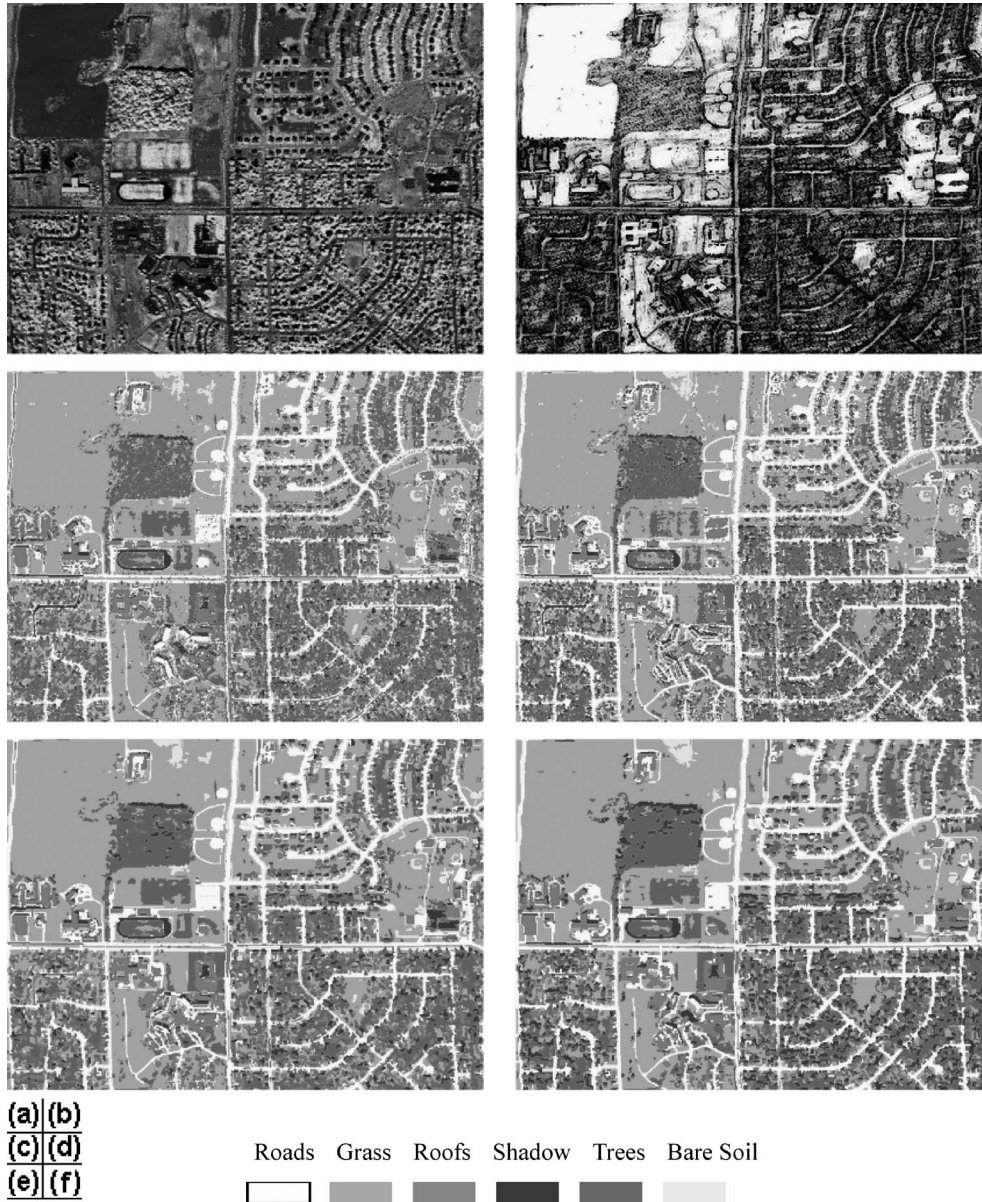
Fig. 11. (a) Three-dimensional NMF features. (b) PSI feature image with light colors representing larger values and more homogeneity. The PSI image is combined with NMF spectral features to produce the classification map in (d) (the algorithm in [23]), and it is also used for adaptive spatial bandwidths of MS procedure in (f). (c)–(f) Classification results of spectral method (80.5%), combination of spectral and spatial features (89.5%), FNEA (90.6%), and MS-based approach (94.4%), respectively.

TABLE VII
NUMBERS OF TRAINING AND TEST SAMPLES
FOR THE HYMAP CAMPUS DATA SET

Information Classes	No. of Training Samples	No. of Test Samples
Roads	73	1,231
Grass	72	1,072
Shadow	49	215
Bare Soil	69	380
Trees	67	1,321
Roofs	74	1,244
Total	404	5,463

TABLE VIII
CLASS-SPECIFIC ACCURACIES OF THE FOUR
CLASSIFICATION MAPS SHOWN IN FIG. 11

	NMF	NMF+PSI	FNEA	MS
Roads	69.5	83.7	87.5	95.3
Grass	92.7	95.6	96.5	97.1
Shadow	85.1	92.6	80.0	85.5
Bare Soil	87.3	91.0	87.7	91.4
Trees	93.2	95.6	97.3	99.3
Roofs	69.2	85.4	84.7	90.8
AA (%)	82.8	90.6	89.0	93.2
OA (%)	80.5	89.5	90.6	94.4

locally homogeneous regions. The bandwidths are determined using a PSI, which denotes the diameter of the homogeneous areas.

Three data sets are employed to test the proposed classification approach. The experiment on the texture image of QuickBird showed that the MS can achieve perfect segmentation and locate edge pixels very accurately, compared to other
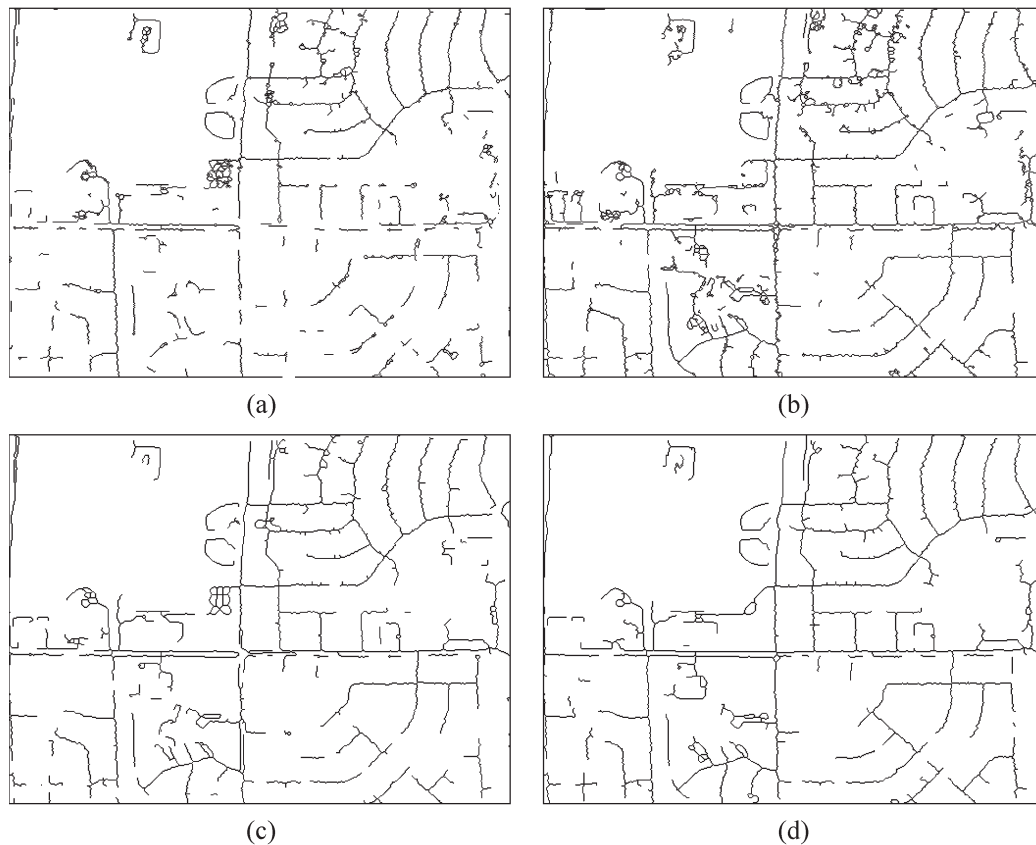
Fig. 12. Road extraction results from the four maps shown in Fig. 11. (a)–(d) Road maps extracted from Fig. 11(c)–(f), respectively.

texture-analysis algorithms such as WT, GLCM, and FNEA segmentation. In the HYDICE, DC experiment, we evaluated the influence of different parameters for the MS procedure, and experimental results showed that the JM index was efficient to detect the optimal range of bandwidths and achieved a satisfactory classification. A comparative study was made between DMP [1], FNEA [17], integration of spectral and the spatial information approach [23], and MS. The MS method obtained the best results in both statistical accuracies and visual interpretation. It is worth noting that the MS approach outperformed FNEA, which is the embedded segmentation algorithm in the eCognition software [17], in all the experiments. The result is promising and verifies the potential of MS for object-oriented classification. Moreover, the same conclusion is obtained with the HYMAP campus data set.

Although the MS-based-analysis approach is with good results obtained, it is still an interesting problem whether the multiscale or multilevel approach is a better solution for VHR images. In the future, we also plan to study the relationship between the dimensionality and MS procedure and make a comparison with other classifiers (e.g., Gaussian mixture model).

ACKNOWLEDGMENT

REFERENCES

[1] J. A. Benediktsson, J. A. Palmason, and J. R. Sveinsson, "Classification of hyperspectral data from urban areas based on extended morphological profiles," *IEEE Trans. Geosci. Remote Sens.*, vol. 43, no. 3, pp. 480–491, Mar. 2005.

[2] Q. Jackson and D. A. Landgrebe, "Adaptive Bayesian contextual classification based on Markov random fields," *IEEE Trans. Geosci. Remote Sens.*, vol. 40, no. 11, pp. 2454–2463, Nov. 2002.

[3] M. M. Dundar and D. A. Landgrebe, "A model-based mixture-supervised classification approach in hyperspectral data analysis," *IEEE Trans. Geosci. Remote Sens.*, vol. 40, no. 12, pp. 2692–2699, Dec. 2002.

[4] K. Fukunaga and L. D. Hostetler, "The estimation of the gradient of a density function, with applications in pattern recognition," *IEEE Trans. Inf. Theory*, vol. IT-21, no. 1, pp. 32–40, Jan. 1975.

[5] D. Comaniciu and P. Meer, "Mean shift: A robust approach toward feature space analysis," *IEEE Trans. Pattern Anal. Mach. Intell.*, vol. 24, no. 5, pp. 603–619, May 2002.

[6] K. Fukunaga, *Introduction to Statistical Pattern Recognition*, 2nd ed. New York: Academic, 1990.

[7] J. A. Palmason, J. A. Benediktsson, J. R. Sveinsson, and J. Chanussot, "Classification of hyperspectral data from urban areas using morphological preprocessing and independent component analysis," in *Proc. IEEE Geosci. Remote Sens. Symp.*, Seoul, Korea, Jul. 25–29, 2005, vol. 6, pp. 176–179.

[8] D. D. Lee and H. S. Seung, "Learning the parts of objects by non-negative matrix factorization," *Nature*, vol. 401, no. 6775, pp. 788–791, Oct. 1999.

[9] *eCognition Professional User Guide 4*, Definiens Imaging, Munich, Germany, 2003. [Online]. Available: http://www.definiens-imaging.com

[10] L. Bruzzone and L. Carlin, "A multilevel context-based system for classification of very high spatial resolution images," *IEEE Trans. Geosci. Remote Sens.*, vol. 44, no. 9, pp. 2587–2600, Sep. 2006.

[11] L. Wang, W. P. Sousa, and P. Gong, "Integration of object-based and pixel-based classification for mapping mangroves with IKONOS imagery," *Int. J. Remote Sens.*, vol. 25, no. 24, pp. 5655–5668, Dec. 2004.

[12] Q. Yu, P. Gong, N. Clinton, G. Biging, and D. Schirokauer, "Object-based detailed vegetation classification with airborne high spatial resolution remote sensing imagery," *Photogramm. Eng. Remote Sens.*, vol. 72, no. 7, pp. 799–811, Jul. 2006.

[13] C. Cortes and V. Vapnik, "Support vector networks," *Mach. Learn.*, vol. 20, no. 3, pp. 273–297, Sep. 1995.

[14] L. Miao and H. Qi, "Endmember extraction from highly mixed data using minimum volume constrained nonnegative matrix factorization," *IEEE Trans. Geosci. Remote Sens.*, vol. 45, no. 3, pp. 765–777, Mar. 2007.

[15] Y. Zhang, "Optimisation of building detection in satellite images by combining multispectral classification and texture filtering," *ISPRS J. Photogramm. Remote Sens.*, vol. 54, no. 1, pp. 50–60, Feb. 1999.

[16] M. Acharyya, R. K. De, and A. K. Kundu, "Segmentation of remotely sensed images using wavelet features and their evaluation in soft computing framework," *IEEE Trans. Geosci. Remote Sens.*, vol. 41, no. 12, pp. 2900–2905, Dec. 2003.

[17] G. J. Hay, T. Blaschke, D. J. Marceau, and A. Bouchard, "A comparison of three image-object methods for the multiscale analysis of landscape structure," *ISPRS J. Photogramm. Remote Sens.*, vol. 57, no. 5, pp. 327–345, Apr. 2003.

[18] X. Huang, L. Zhang, and P. Li, "An adaptive multiscale information fusion approach for feature extraction and classification of IKONOS multispectral imagery over urban areas," *IEEE Geosci. Remote Sens. Lett.*, vol. 4, no. 4, pp. 654–658, Oct. 2007.

[19] Q. Luo and M. Khoshgoftaar, "Unsupervised multiscale color image segmentation based on MDL principle," *IEEE Trans. Image Process.*, vol. 15, no. 9, pp. 2755–2761, Sep. 2006.

[20] D. Comaniciu, "An algorithm for data-driven bandwidth selection," *IEEE Trans. Pattern Anal. Mach. Intell.*, vol. 25, no. 2, pp. 281–288, Feb. 2003.

[21] J. A. Richards and X. Jia, *Remote Sensing Digital Image Analysis: An Introduction.* Berlin, Germany: Springer-Verlag, 1999.

[22] L. Bruzzone, F. Roli, and S. B. Serpico, "An extension of the Jeffreys–Matusita distance to multiclass cases for feature selection," *IEEE Trans. Geosci. Remote Sens.*, vol. 33, no. 6, pp. 1318–1321, Nov. 1995.

[23] L. Zhang, X. Huang, B. Huang, and P. Li, "A pixel shape index coupled with spectral information for classification of high spatial resolution remotely sensed imagery," *IEEE Trans. Geosci. Remote Sens.*, vol. 44, no. 10, pp. 2950–2961, Oct. 2006.

[24] D. A. Landgrebe, *Signal Theory Methods in Multispectral Remote Sensing.* Hoboken, NJ: Wiley, 2003.

[25] P. Gamba, F. Dell'Acqua, G. Lisini, and G. Trianni, "Improved VHR urban area mapping exploiting object boundaries," *IEEE Trans. Geosci. Remote Sens.*, vol. 45, no. 8, pp. 2676–2682, Aug. 2007.

[26] Z. Wang and R. Boesch, "Color- and texture-based image segmentation for improved forest delineation," *IEEE Trans. Geosci. Remote Sens.*, vol. 45, no. 10, pp. 3055–3062, Oct. 2007.

[27] R. L. Kettig and D. A. Landgrebe, "Classification of multispectral image data by extraction and classification of homogeneous objects," *IEEE Trans. Geosci. Electron.*, vol. GE-14, no. 1, pp. 19–26, Jan. 1976.

[28] D. A. Landgrebe, "The development of a spectral–spatial classifier for earth observational data," *Pattern Recognit.*, vol. 12, no. 3, pp. 165–175, 1980.

[29] B. Waske and J. A. Benediktsson, "Fusion of support vector machines for classification of multisensor data," *IEEE Trans. Geosci. Remote Sens.*, vol. 45, no. 12, pp. 3858–3866, Dec. 2007.
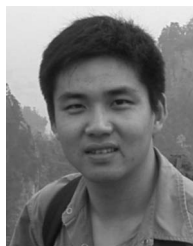
Xin Huang received the B.S. and M.S. degrees in sciences and techniques of remote sensing from Wuhan University, Wuhan, China, in 2004 and 2006, respectively, and the Ph.D. degree in sciences and techniques of remote sensing from the State Key Laboratory of Information Engineering in Surveying, Mapping and Remote Sensing (LIESMARS), Wuhan University, in 2009.

He is currently with LIESMARS, Wuhan University. His research interests include hyperspectral data analysis, high-resolution image processing, pattern recognition, and remote-sensing applications.

Dr. Huang was a Referee of the 2008 IEEE International Geoscience and Remote Sensing Symposium and *Photogrammetric Engineering and Remote Sensing*. He is the first author of eight scientific publications in refereed international journals such as IEEE TRANSACTIONS ON GEOSCIENCE AND REMOTE SENSING, IEEE GEOSCIENCE AND REMOTE SENSING LETTERS, *Photogrammetric Engineering and Remote Sensing* and *International Journal of Remote Sensing*. From 2004 to 2008, he ranked the first place in the outstanding graduate student in LIESMARS, Wuhan University. In 2008, he was the recipient of the Trimble Scholarship from Trimble Navigation Limited Company.

Liangpei Zhang received the B.S. degree in physics from Hunan Normal University, ChangSha, China, in 1982, the M.S. degree in optics from Xi'an Institute of Optics and Precision Mechanics, Chinese Academy of Sciences, Xi'an, China, in 1988, and the Ph.D. degree in photogrammetry and remote sensing from Wuhan University, Wuhan, China, in 1998.

From 1997 to 2000, he was a Professor with the School of the Land Sciences, Wuhan University. Since August 2000, he has been with the State Key Laboratory of Information Engineering in Surveying, Mapping and Remote Sensing, Wuhan University, where he has been a Professor and the Head of the Remote Sensing Section. Since 2007, he has been nominated as a "ChangJiang Scholar" Professor (Chair Professor) by the Education Ministry of China. He has published more than 150 research papers. His research interests include hyperspectral remote sensing, high-resolution remote sensing, image processing, and artificial intelligence.

Dr. Zhang has served as Cochair of the International Society for Optical Engineers Series Conferences on Multispectral Image Processing and Pattern Recognition (MIPPR) and of the Conference on Asia Remote Sensing in 1999. He was the Editor of the MIPPR01, MIPPR05, and Geoinformatics Symposiums, the Associate Editor of *Geo-spatial Information Science Journal*, Chinese National Committee for the International Geosphere–Biosphere Programme, and an executive member for the China Society of Image and Graphics.